3D range-modulators for proton therapy: near field simulations with FLUKA and comparison with film measurements

3D range-modulators for proton therapy: near field simulations with FLUKA and comparison with film measurements

W Charuchinda[1,2], F Horst[2], Y Simeonov[3], C Schuy[2], P Penchev[3], P Poulsen[4], M Sitarz[4], S Busold[5], C-A Reidel[2], M Folkerts[6], M Krieger[5], N Suwonjandee[1], B Asavapibhop[1], M Durante[2], K Zink[3] and U Weber[2,*]

[1] Department of Physics, Chulalongkorn University, Bangkok, Thailand
[2] Biophysics Division, GSI Helmholtzzentrum für Schwerionenforschung, Darmstadt, Germany
[3] Institut für Medizinische Physik und Strahlenschutz, Technische Hochschule Mittelhessen, Giessen, Germany
[4] Danish Center for Particle Therapy (DCPT), Aarhus, Denmark
[5] Varian Medical Systems Particle Therapy, Troisdorf, Germany
[6] Varian Medical Systems, Inc., Palo Alto, California, USA

*Email: U.Weber@gsi.de

Abstract. The 3D range-modulator is a device used in particle delivery systems that can create a highly conformal and homogeneous dose distribution in the target volume with mono-energetic beams, providing an option for high dose-rate FLASH therapy. In the normal case, the modulators are positioned at a typical distance of 30-50 cm in front of the target in order to avoid the fluence ripples resulting from the periodic structure of the modulators. FLUKA Monte Carlo simulation package was used to investigate the fluence distributions of protons penetrating through the 2D range-modulator, the simplified version of the 3D range-modulator, and to determine the minimum distance at which the fluence is homogeneous enough for the treatment. To implement the complex geometry of the modulator in FLUKA, a dedicated FLUKA user routine was developed for the simulation of the periodic pin structures. The highest fluence ripple occurred at a few centimetres behind the modulators and then faded away as the distance increased, which can be described by the edge-scattering effect and later by the blur-out of the overlapping contributions from the pins. Moreover, the dose distribution in water was investigated, particularly for small distances between the modulators and the water phantom. Furthermore, the Monte Carlo results were compared with radiochromic film measurements irradiated with a 3D-printed range modulator and showed a good qualitative agreement. Prospectively, for low modulator-to-target distances, the strong dose inhomogeneities which appear in the proximal part of the target, could introduce additionally a kind of 'mini beam' normal-tissue sparing by the 3D range-modulators.

1. Introduction

A 3D range-modulator (3D-RM) [1,2] is a 3D-printed passive device that prospectively can be used for very fast irradiations in proton or heavy-ion therapy [3,4]. The device is a combination of a range

compensator and a ripple filter [5], which consists of many different pyramid structures (pins) with a well-defined profile that is optimized to deliver a conformal dose in a specific target volume [1,2] (Figure 1(a)). In combination with the raster scanning technique, the 3D-RM creates a conformal and homogeneous dose distribution in the target volume by irradiating with only one energy. In contrast to the standard multi energy-layer raster scanning [6,7], this method provides a much shorter total irradiation time due to the absence of the 'dead time' that the beam delivery machine needs to change the energy. Consequently, it can enable FLASH irradiations [8-11] and fast treatment for moving targets (<<1 s), e.g., for lung and liver cancer. With consistent research and development, the 3D-RMs are promising for clinical application in the near future.

A particular effect induced by the periodic fine structure of the modulator in ion beam therapy is the inhomogeneous fluence in the near field region [12]. Because it might cause strong dose inhomogeneities on the skin, in the proximal normal tissue or even in the target volume, modulators are normally placed far away from the target. However, the inhomogeneity induced by 3D-RM has never been systematically investigated before. Thus, in this work, film measurements and Monte Carlo simulations were performed to specifically observe the behavior of such inhomogeneities for the purpose that the usage of the 3D-RM can be optimized. In this work, for better systematics, we used a simplified version of the 3D-RM, a so-called 2D range-modulator (2D-RM) [13], in which all pins have the same shape and height as shown in figure 1(b).

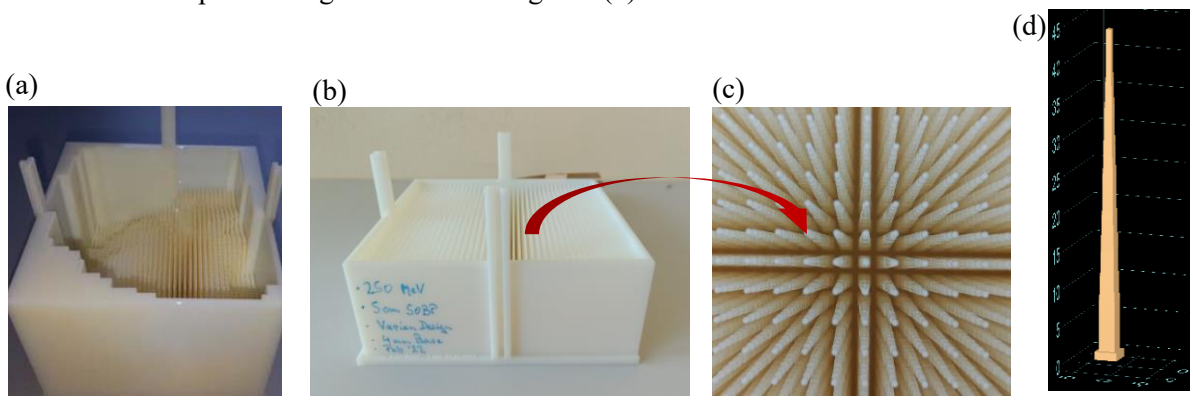

Figure 1. Examples of (a) a 3D-RM [2], (b) a 2D-RM, (c) a close look of the pin's fine structures, and (d) a single pin of the 2D-RM.

2. Material and method

2.1. 2D range-modulator (2D-RM)

The 2D-RM is a special kind of the 3D-RM that is used for creating a Spread-Out Bragg Peak (SOBP) in the target. Rather than being used in the clinics for treating patients, the 2D-RMs are more likely designed for research purposes providing the versatility of their usage. In this work, we used the 2D-RM that is composed of identical pins (see figures 1(c) and 1(d)) with a 3×3 mm^2 base and 44 mm height. The device was designed in earlier work for 250 MeV proton beams to create a 5 cm SOBP [13]. A Stratasys Objet30-Pro 3D-printer and a propriety material (RIGUR RGD450, Stratasys) were used for manufacturing the modulator. Its composition is similar to Polypropylene and has a density of 1.2 g/cm^3.

2.2. Gafchromic EBT-3 film measurements

The film measurements were performed at the Danish Centre for Particle Therapy (DCPT) at Aarhus University Hospital, Denmark. The experimental setup is shown in figure 2 where the *ProBeam*® proton therapy system from *Varian Medical Systems* was used for generating and delivering the beam to the target. The beam passed through an ionization chamber (IC), the 2D-RM, PMMA absorber plates of 19 cm total thickness, and was stopped in a water phantom [14]. The front window of the

water phantom was positioned at the isocenter plane and the 2D-RM was positioned 25.5 cm upstream of the isocenter.

The films were irradiated with a beam of 250 MeV protons having a pencil-beam width of roughly 8 mm FWHM at the modulator position. A homogeneous quadratic field was scanned by a pattern of 10×10 beam spots with 6 mm step size, yielding 10 Gy dose in the middle of SOBP. Additionally, the intensities of the beam spots at the border were slightly boosted-up by 5% in order to sharpen the lateral fall-off.

Radiochromic films (Gafchromic EBT-3) were placed at different distances behind the modulator to observe the development of the inhomogeneities. The film1 was attached to the front of the modulator. The other films were attached to the energy absorbers where the distances from the modulator of film2 to film6 were 3.4, 7.1, 12.1, 17.1, and 25.5 cm, respectively. After irradiation, all films were scanned with an *Epson Expression 12000XL Pro scanner* with a resolution of 72 ppi.

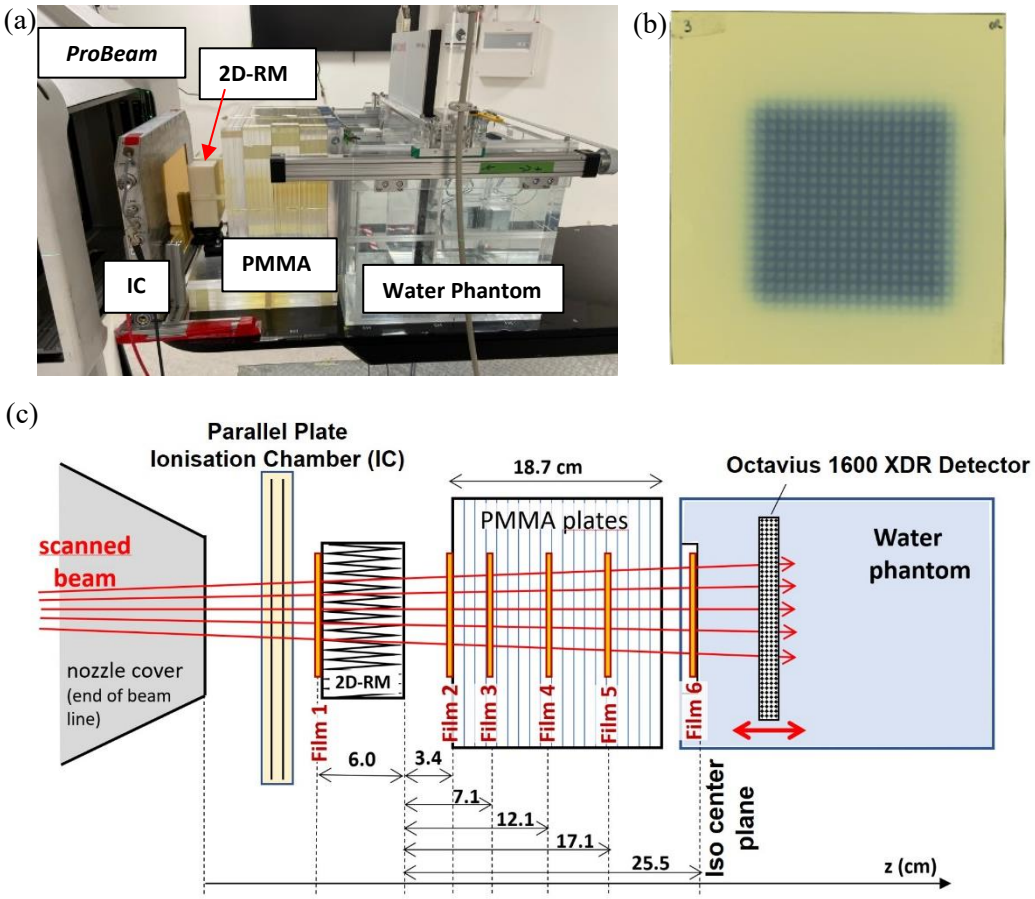

Figure 2. (a) Experimental setup at DCPT, (b) an example of irradiated radiochromic films (*Gafchromic EBT-3)* at a position of 7.1 cm behind the modulator, with a visible ripple effect, and (c) a schematic drawing of the experimental setup with the film positions.

2.3. Comparison with Monte Carlo simulation FLUKA

The film measurements were compared with simulations using the Monte Carlo simulation package FLUKA version 2020.0.10 [15,16] which is a multi-purpose particle transport code developed by CERN and INFN. FLUKA is in Europe one of the most common Monte Carlo programs for particle therapy, in particular for creating base data for treatment planning systems [17]. To perform our simulation, the simplified geometries, and the physical properties of the materials of the experimental devices were inserted in the FLUKA standard input file, except for the 2D-RM which was

implemented with the help of a special USRMED.f routine (see section 2.4) due to the complexity of its geometry. The FLUKA geometrical setup corresponds to the experimental setup. The z-axis represents the beam direction, z = 0 cm is the beam origin (scanner magnets x), and z = 200 cm is the position of the isocenter. A 1 mm homogeneous water slab was added as a water equivalent nozzle substitute and was placed at the position of the exit window.

The beam configuration was the same as used in the experiment, essentially, the magnetic scanning deflection was also considered. To calculate the deflection angle of the beams, the information regarding the *ProBeam*® machine was provided by *Varian Medical Systems*.

The lateral fluence distributions in the unit of particles/cm^2 per primary weight were scored at the virtual positions of the films using a USRBIN card. The total scoring size was 80×80×0.03 mm^3 (x y z) with one bin in the z-direction and 600 bins in both x- and y-directions. 5×10^9 primary protons were generated in the simulation and the running jobs were sent to the FLUKA cluster of GSI to utilize 100 CPUs.

2.4. 2D range-modulator implementation in FLUKA

The USRMED.f routine was customized and written in FORTRAN77 to implement the complex shape of the 2D-RM in FLUKA. It is similar to the concept described in [1]. To call the USRMED.f via the MAT-PROP card, a homogeneous "substitute" plate with the same material as the 2D-RM was added to the FLUKA standard input. Importantly, the thickness of the substitute plate needs to be equal to the maximum height of the actual modulator. Then, every time when a particle hits this plate, the USRMED.f routine will be activated and shifts the particle along its directional vector, from its initial position, (x, y, z) for the example in figure 3(a), until reaching the modulator. After that the final coordinates (x´, y´, z´) will be sent back to FLUKA and the absolute authority will be returned to FLUKA executable again.

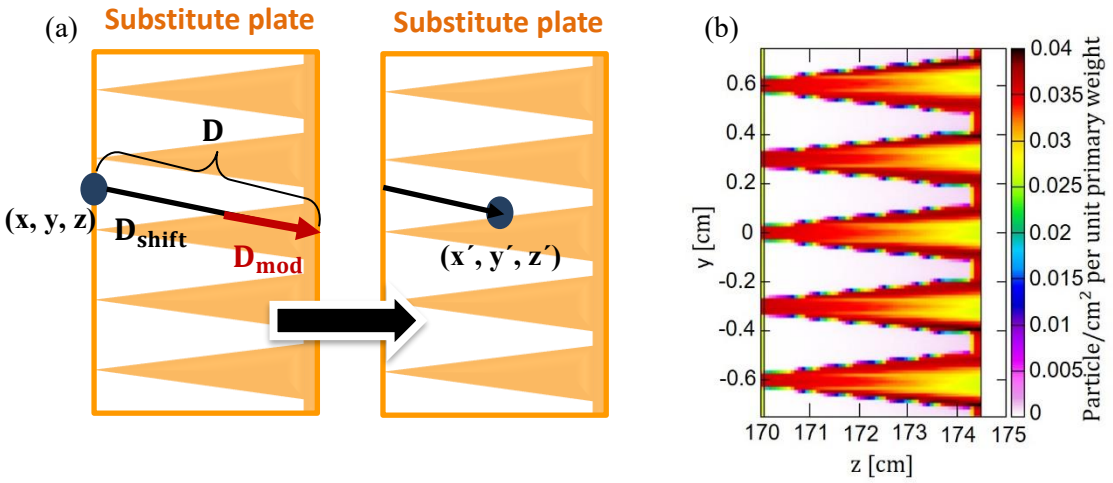

Figure 3. (a) The demonstration of the particle shifting through the substitute plate to realize the shape of the 2D-RM and (b) the 2D fluence color plot at the substitute plate when using the USRMED.f routine.

Before shifting the particle, one has to calculate the distance that the particle will travel in the modulator (D_{mod}). For this purpose, the profile of 2D-RM pins was saved in an input file (as a set of interpolation points with the pin height as a function of the pin radius), which will be called by the routine during the first entry of the particle. It should be noted, that in this work, we changed the algorithm to calculate the D_{mod} from "the ray-triangle intersection algorithm" [1,2] to this faster but less flexible method using interpolation points for the profile instead of a full STL-data set. After the calculation of the D_{mod}, the distance of the particle shifting (D_{shift}) was calculated by the subtraction of

the D_{mod} from the total distance D that the particle passes through the substitute plate. Then, the particle would be translated along its directional vector with the distance of D_{shift}.

Figure 3(b) shows an example for color wash map of the proton fluence zoomed to the substitute plate which shows the realization of the shape of the 2D-RM by using the USRMED.f routine. The white spaces indicate the absence of the particles since they were shifted directly to the modulator by the USRMED.f routine.

3. Results and discussion

The lateral fluctuations (oscillation) of the fluence are caused by the strongly inhomogeneous scattering at the periodic structures of the modulator [12]. The comparison of the 2D fluence profiles from simulations and measurements is shown in figure 4. The 2D fluence distribution (in x-z plane) and the strength of the fluence oscillation in dependency from z are shown in figure 5. It can be seen that the fluence is focused (increased) at the positions of the pin's grooves (lower scattering) and decreased behind the pin's peaks (stronger scattering). However, the contributions from the single pins are overlapping at larger distances behind the modulator and therefore regaining homogeneity. The strength of such a fluence inhomogeneity is influenced by the edge-scattering effect which was studied thoroughly by the research of the dose perturbation induced by fiducial markers [18-20].

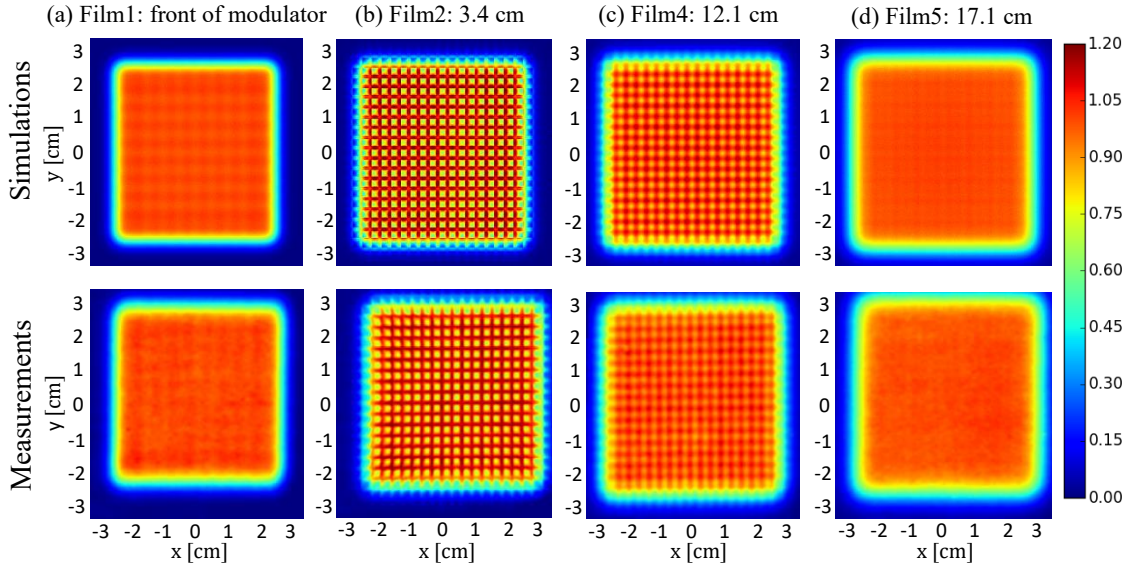

Figure 4. 2D fluence profiles from the FLUKA simulations (top) and film measurements (bottom) for (a) film1, (b) film2, (c) film4, and (d) film5.

For quantitative comparison, the inhomogeneities at different distances were quantified as a numerical value which is called "fluence ripple (R)" and can be calculated by

$$R = \frac{F_{max} - F_{min}}{F_{max} + F_{min}}. \quad (1)$$

F_{max} and F_{min} are the maximum and the minimum fluence at the 5×5 mm^2 squared region in the middle of the field. To search for F_{max} and F_{min}, the measured and simulated fluence distributions were fitted by an oscillating fit function. Thus, the fluence ripple in percentage was plotted against the distances as shown in figure 5(b).

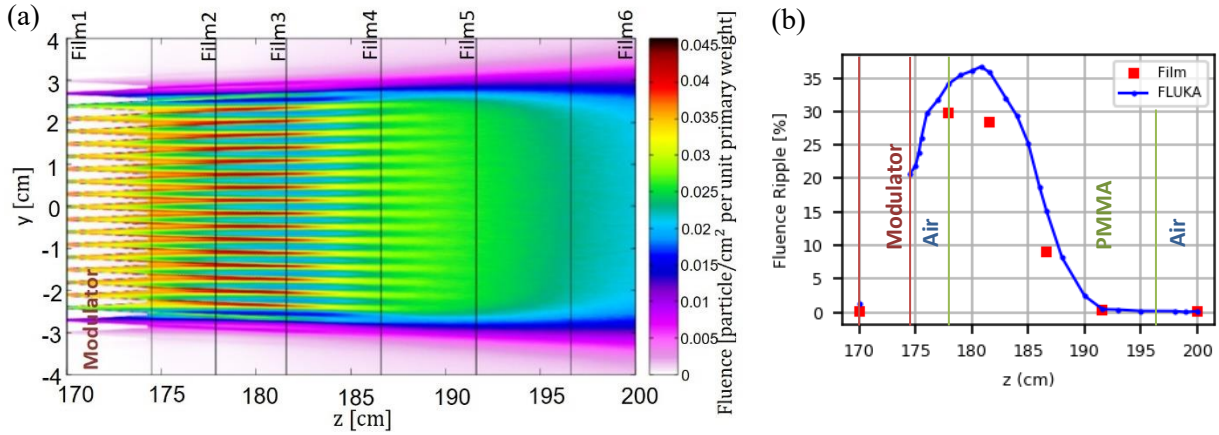

Figure 5. Inhomogeneities of the near field behind the modulator spotted in (a) 2D fluence color plot and represented as (b) the fluence ripple function.

The measurement results in figure 4 and figure 5 show that the strongest inhomogeneity appeared on the closest film to the modulator (film2) with a fluence ripple of 29.8%, then decreased and completely blurred out at the position of the film5 or 17.1 cm behind the modulator which can ensure the homogenous field at the isocenter. The simulations agreed with the measurements and revealed the actual location of the maximum inhomogeneity with the ripple of 36.7% which was between the film2 and the film3 or around 6.3 cm behind the modulator. We suspect two reasons for the deviations in the magnitude of the simulated and measured inhomogeneities: Firstly, the lower resolution of the scanned films data, and secondly a possibly wider angular distribution from the beamline and the nozzle.

Nevertheless, the most relevant is to know the qualitative development as a function of the depth and to validate at which depth the ripple has completely blurred-out.

Apart from the dependence on the distance, further investigation by using FLUKA also shows that the inhomogeneity is sensitive to the beam parameters such as the beam energy and the angular distribution as shown in figure 6(a) and figure 6(b), respectively. We observed a strong dependence of

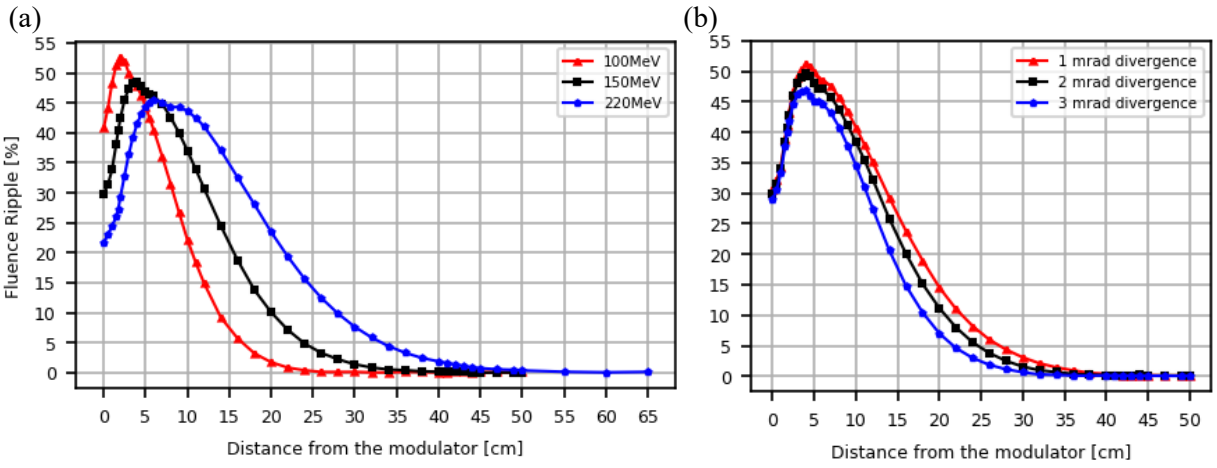

Figure 6. The fluence ripple function with the variation of (a) the beam energy and (b) the beam divergence.

the fluence ripple in the beam energy. Since the protons with higher energy have more capability to keep traveling forward in their original direction or scatter with smaller angles according to highland's formula [21,22], the scattered contributions overlap at further distances from the modulator. For 220 MeV protons, the minimum distance that can guarantee complete homogeneity is 50 cm, which is

considerably larger than the minimum distance of about 30 cm for 100 MeV protons. The increase of the initial beam divergence also reduces the strength of the inhomogeneity because the larger angular dispersion decreases particle focusing. However, the deviations of the minimum distances are small (< 6 cm) when compared to the sensitivity to the beam energy.

As mentioned before, an inhomogeneous field is usually unwanted in the case of conventional treatment plans. However, the research on minibeam particle therapy [23] implies the possibility to exploit such a strong dose inhomogeneity for sparing the normal tissue. Figure 7 shows the simulated dose distribution in the water phantom when the modulator was placed at a distance of 2 cm in front of the water surface, noted that the water was positioned at the virtual isocenter or at z = 200 cm in FLUKA. By performing this way, the lateral dose (resp. fluence) ripple is presented on the patient's skin and also penetrates for several centimetres into the normal tissue, whereas in the target volume it is blurred-out again. This allows the hypothesis that this kind of strong dose ripple might have a positive "minibeam effect" on the skin and the proximal normal tissue, or at least no deterioration compared to a homogeneous dose application. Figure 7(b) and figure 7(c) show lateral dose distributions at the water surface where figure 7(c) is the dose profile at x = 0 cm. The peak and valley of dose were spotted in a similar manner to minibeam which the Peak-to-Valley Ratios (PVDR) at the first 4 cm of the water are between the factor of 2 and 3. However, they are lower than what they normally have been in minibeam studies. Clearly, in order to verify this kind of 'soft-minibeam effect', the biological response needs to be investigated in pre-clinical experiments with animals. If this hypothesis turned out to be true, it would have a second advantage, because the closer distance of the modulator to the patient would reduce the scattering effect by the modulator and therefore improve the dose conformity to the tumour.

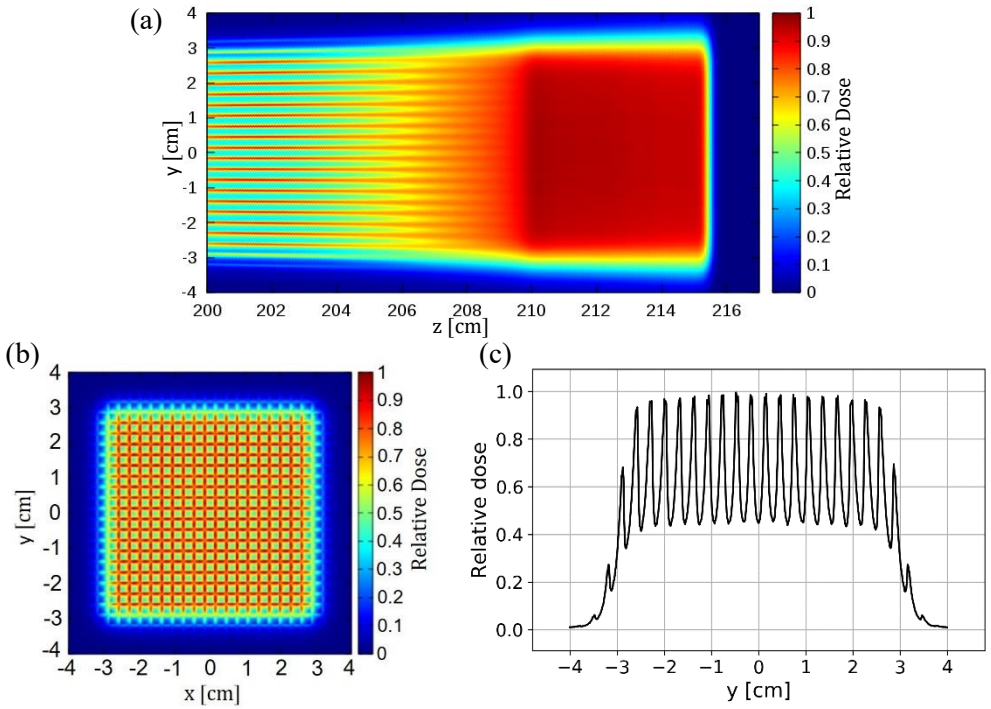

Figure 7. Simulated dose inhomogeneities (a) in 2D depth dose distribution, (b) at the water surface and (c) the dose profile at x = 0 cm when the modulator is placed 2 cm in front of the water.

4. Conclusion

The 3D-RM is a dose-modulating device used in particle therapy to create a conformal dose distribution in a target volume within a very short irradiation time (<<1 s) thus enabling FLASH irradiation [2]. In this study, the inhomogeneities of the beam field induced by the modulator were

investigated by radiochromic film measurements and FLUKA simulations for proton beams. The results show a good qualitative agreement The inhomogeneities and their dependence on the modulator distance could be well reproduced by the simulations. The maximum fluence ripple appears 5-10 cm behind the modulator, however, for 100 MeV at 20 cm distance, for 150 MeV at 30 cm distance, and for 220 MeV at 50 cm distance from the modulator, the ripple should have disappeared. However, if one intentionally places the modulator very close to the skin, a strong dose-ripple is induced into the normal tissue. Although an inhomogeneous field is usually avoided in the normal treatment plan, such a strong dose inhomogeneity might introduce a kind of 'mini beam' normal-tissue sparing. Nevertheless, the biological effect of the dose-ripple would still need to be investigated in animal experiments.

References

[1] Simeonov Y, Weber U, Penchev P, Ringbæk T P, Schuy C, Brons S, Engenhart-Cabillic R, Bliedtner J and Zink K 2017 *Phys. Med. Biol.* **62** 7075–96
[2] Simeonov Y, Weber U, Schuy C, Engenhart-Cabillic R, Penchev P, Flatten V and Zink K 2022 *Biomed. Phys. Eng. Express* **8** 035006
[3] Newhauser W D and Zhang R 2015 *Phys. Med. Biol.* **60** R155–209
[4] Schardt D, Elsässer T and Schulz-Ertner D 2010 *Rev. Mod. Phys.* **82** 383–425
[5] Weber U and Kraft G 1999 *Phys. Med. Biol.* **44** 2765–75
[6] Haberer T, Becher W, Schardt D and Kraft G 1993 *Nucl. Instrum. Methods Phys. Res.* A **330** 296–305
[7] Pedroni E *et al* 1995 *Med. Phys.* **22** 37–53
[8] Weber U A, Scifoni E and Durante M 2022 *Med. Phys.* **49** 1974–92
[9] Tinganelli W *et al* 2022 *Int. J. Radiat. Oncol. Biol. Phys.* **112** 1012–22
[10] Favaudon V *et al* 2014 *Sci. Transl. Med.* **6** 245ra93
[11] Durante M, Bräuer-Krisch E and Hill M 2018 *Br. J. Radiol.* **91** 20170628
[12] Ringbæk T P, Weber U, Petersen J B, Thomsen B and Bassler N 2014 *Acta Oncol.* **53** 40–9
[13] Simeonov Y, Weber U, Schuy C, Engenhart-Cabillic R, Penchev P, Durante M and Zink K 2021 *Z. Med. Phys.* **31** 203–14
[14] Schuy C, Simeonov Y, Durante M, Zink K and Weber U 2020 *J. Appl. Clin. Med. Phys.* **21** 227–32
[15] Ferrari A, Sala P R, Fassò A and Ranft J 2005 *FLUKA: A Multi-Particle Transport Code (Program Version 2005)* (Geneva: CERN) (https://doi.org/10.2172/877507)
[16] Böhlen T T, Cerutti F, Chin M P W, Fassò A, Ferrari A, Ortega P G, Mairani A, Sala P R, Smirnov G and Vlachoudis V 2014 *Nucl. Data Sheets* **120** 211–4
[17] Parodi K, Mairani A, Brons S, Hasch B G, Sommerer F, Naumann J, Jäkel O, Haberer T and Debus J 2012 *Phys. Med. Biol.* **57** 3759–84
[18] Newhauser W D, Fontenot J, Koch N, Dong L, Lee A, Zheng Y, Waters L and Mohan R 2007 *Phys. Med. Biol.* **52** 2937–52
[19] Cheung J, Kudchadker R J, Zhu X R, Lee A K and Newhauser W D 2010 *Phys. Med. Biol.* **55** 7135–47.
[20] Reidel C-A, Horst F, Schuy C, Jäkel O, Ecker S, Henkner K, Brons S, Durante M and Weber U 2022 *Front. Oncol.* **12** 830080
[21] Highland V L 1975 *Nucl. Instr. Meth.* **129** 497–9
[22] Highland V L 1979 *Nucl. Instr. Meth.* **161** 171
[23] Meyer J, Eley J, Schmid T E, Combs S E, Dendale R and Prezado Y 2019 *Br. J. Radiol.* **92** 20180466